

Tunable anomalous Hall effect and anisotropic magnetism in In-doped $TbMn_6Sn_6$ kagome magnets

Detong Wu(吴德桐), Jianwei Qin(秦建伟), and Bing Shen(沈冰)

Citation: Chin. Phys. B, 2025, 34 (**10**): 107511. DOI: 10.1088/1674-1056/adde37
http://cpb.iphy.ac.cn; http://iopscience.iop.org/cpb

What follows is a list of articles you may be interested in

Anomalous Hall effect and electronic correlation in a spin-reoriented kagome antiferromagnet $LuFe_6Sn_6$

Meng Lyu(吕孟), Yang Liu(刘洋), Shen Zhang(张伸), Junyan Liu(刘俊艳), Jinying Yang(杨金颖), Yibo Wang(王一博), Yiting Feng(冯乙婷), Xuebin Dong(董学斌), Binbin Wang(王彬彬), Hongxiang Wei(魏红祥), and Enke Liu(刘恩克)

Chin. Phys. B, 2024, 33 (**10**): 107507. DOI: 10.1088/1674-1056/ad6f93

Evolution of anomalous Hall effect in ferromagnetic Weyl semimetal $Nb_xZr_{1-x}Co_2Sn$

Bo-Wen Chen(陈博文) and Bing Shen(沈冰)

Chin. Phys. B, 2024, 33 (**8**): 087501. DOI: 10.1088/1674-1056/ad4a3b

Tailoring-compensated ferrimagnetic state and anomalous Hall effect in quaternary Mn-Ru-V-Ga Heusler compounds

Jin-Jing Liang(梁瑾静), Xue-Kui Xi(郗学奎), Wen-Hong Wang(王文洪), and Yong-Chang Lau(刘永昌)

Chin. Phys. B, 2024, 33 (**7**): 077504. DOI: 10.1088/1674-1056/ad34c8

Enhanced anomalous Hall effect in kagome magnet $YbMn_6Sn_6$ with intermediate-valence ytterbium

Longfei Li(李龙飞), Shengwei Chi(迟晟玮), Wenlong Ma(马文龙), Kaizhen Guo(郭凯臻), Gang Xu(徐刚), and Shuang Jia(贾爽)

Chin. Phys. B, 2024, 33 (**5**): 057501. DOI: 10.1088/1674-1056/ad322d

Angular and planar transport properties of antiferromagnetic V_5S_8

Xiao-Kai Wu(吴晓凯), Bin Wang(王彬), De-Tong Wu(吴德桐), Bo-Wen Chen(陈博文), Meng-Juan Mi(弭孟娟), Yi-Lin Wang(王以林), and Bing Shen(沈冰)

Chin. Phys. B, 2024, 33 (**2**): 027503. DOI: 10.1088/1674-1056/ad15f9

Tunable anomalous Hall effect and anisotropic magnetism in In-doped $TbMn_6Sn_6$ kagome magnets

Detong Wu(吴德桐)[1,2,†], Jianwei Qin(秦建伟)[1,2,†], and Bing Shen(沈冰)[1,2,‡]

[1] *Center for Neutron Science and Technology, Guangdong Provincial Key Laboratory of Magnetoelectric Physics and Devices, School of Physics, Sun Yat-Sen University, Guangzhou* 510275, *China*

[2] *State Key Laboratory of Optoelectronic Materials and Technologies, Sun Yat-Sen University, Guangzhou* 510275, *China*

(Received 7 April 2025; revised manuscript received 28 May 2025; accepted manuscript online 29 May 2025)

Kagome magnets $TbMn_6Sn_{6-x}In_x$ ($x = 0$–1.2) exhibit a robust anomalous Hall effect (AHE) that persists above room temperature, demonstrating significant potential for high-temperature spintronics applications. At elevated temperatures, a spin-reorientation transition induces a ferrimagnetic state (FIM1) with in-plane magnetic moments, accompanied by a non-monotonic Hall response that differs markedly from the low-temperature behavior. Upon indium doping, the long-range ferrimagnetic transition is progressively suppressed to lower temperatures, along with a noticeable reduction in magnetic anisotropy. Interestingly, at a doping level of $x = 1.2$, the FIM1 state observed in the parent compound is completely eliminated. These systematic changes in magnetic ordering and transport properties underscore a coherent evolution of the electronic and magnetic states with doping, offering critical insights into the interplay among lattice structure, magnetism, and electronic behavior in kagome lattices.

Keywords: anomalous Hall effect, magnetic properties, ferrimagnetism, nonmagnetic element doping

PACS: 72.20.My, 75.30.Kz, 75.30.Cr, 75.50.Gg

DOI: 10.1088/1674-1056/adde37 **CSTR:** 32038.14.CPB.adde37

1. Introduction

Kagome lattice consists of corner-sharing triangles arranged in a two-dimensional plane, forming a distinctive tiling pattern of regular hexagons and equilateral triangles.[1] This unique geometric configuration imparts high symmetry to the lattice, resulting in a characteristic electronic band structure with a dispersionless flat band and two linearly dispersing Dirac bands.[2–6] Introducing magnetism into kagome materials creates an interplay between their magnetic and electronic structures, giving rise to a range of exotic physical phenomena. The RMn_6Sn_6 family of compounds represents a class of prototypical kagome magnets, where Mn atoms form a pristine kagome lattice within the plane, offering an ideal platform for exploring the intrinsic electronic band properties of kagome systems. Magnetic order and anisotropy in these materials are highly sensitive to the choice of rare earth element (R).[7–10] For example, R = Sc, Y, Er, Tm, and Lu lead to antiferromagnetic order with Néel temperatures exceeding room temperature, while R = Gd, Tb, Dy, and Ho result in ferromagnetic or ferrimagnetic (FIM) ordering with Curie temperatures ranging from 376 K to 435 K.[11,12] Regarding anisotropy, $DyMn_6Sn_6$ and $HoMn_6Sn_6$ exhibit easy-cone anisotropy with a cone angle of approximately 45° at low temperatures,[13] while $TbMn_6Sn_6$ displays easy-axis anisotropy along the c-axis in its ground state. By manipulating the magnetic elements (e.g., rare-earth substitutions), the magnetic structure can be effectively tuned to engineer potential Chern quantum phases in kagome magnets.[14]

Among these kagome magnets, $TbMn_6Sn_6$ stands out due to its pristine kagome lattice (free of interstitials within the kagome plane) and robust out-of-plane magnetization that persists above room temperature, aligning with the Haldane model for hosting Chern-gapped Dirac fermions.[12,15–18] Additionally, $TbMn_6Sn_6$ exhibits temperature-dependent magnetic anisotropy and a rich magnetic phase diagram. It demonstrates easy-plane anisotropy within the ab-plane between its Curie temperature ($T_C \sim 425$ K) and spin-reorientation temperature ($T_{SR} \sim 300$ K), followed by a transition to easy-axis anisotropy along the c-axis below 300 K.[19,20] This crossover arises from the increasing dominance of the magnetic anisotropy of the Tb sublattice at lower temperatures.[21–24] These distinct magnetic states are expected to host different topological phases. The rich phase diagram suggests a complex interplay between magnetism and electronic states, which still remains poorly understood. Previous studies have primarily focused on engineering magnetic elements to induce significant changes in the magnetic structure and electronic states.[25–31] In this study, we take the approach by manipulating non-magnetic elements to control magnetic cor-

[†]These authors contributed equally to this work.

[‡]Corresponding author. E-mail: shenbing@mail.sysu.edu.cn

© 2025 Chinese Physical Society and IOP Publishing Ltd. All rights, including for text and data mining, AI training, and similar technologies, are reserved.

relations while minimizing disruption to the intrinsic magnetic framework. The electronic and magnetic properties of $TbMn_6Sn_{6-x}In_x$ ($x = 0$–1.2) are investigated. By substituting non-magnetic indium into the Sn sites, long-range FIM order is suppressed, and the FIM1 state observed in the parent compound is completely eliminated eventually. The giant anomalous Hall effect and anisotropic magnetization exhibit systemic evolution behavior, suggesting a tunable correlation between the magnetism and electronic state by indium doping.

2. Experimental methods

Single crystals of $TbMn_6Sn_{6-x}In_x$ ($x = 0$–1.2) were grown by using the self-flux method. High-purity terbium (Tb) metal, manganese (Mn) powder, tin (Sn) powder, and indium (In) powder were thoroughly mixed in a molar ratio of $1 : 6 : 30 - 5x : 5x$ and the mixture was packed into an alumina crucible inside an argon-filled glove box. The crucible was sealed in an evacuated quartz ampoule, placed in a box furnace, and heated to 1373 K to ensure a complete reaction. The temperature then slowly cooled down to 823 K, after which the ampoule was promptly removed and centrifuged to separate the flux. As a result, several millimeter-sized hexagonal crystals were obtained. The crystal structure was confirmed by x-ray diffraction (XRD) at room temperature. The selected single crystals were shaped into a rectangular slice for electrical and magnetic transport measurements. Six gold contacts were made on the *ab*-plane with the current along the *a*-axis of the crystals, as shown in Fig. 1(e). Electrical transport measurements were performed in a physical properties measurement system (PPMS Dynacool, Quantum Design). Magnetization measurements were performed by using a superconducting quantum interference device (SQUID) magnetometer.

3. Results and discussion

Figure 1(a) presents the XRD patterns for The $TbMn_6Sn_{6-x}In_x$ ($x = 0$–1.2). The sharp peaks (00l) confirm the high quality of the synthesized crystals. The $TbMn_6Sn_{6-x}In_x$ compounds crystallize in the hexagonal $HfFe_6Ge_6$-type structure, characterized by a layered architecture with Mn atoms forming a kagome lattice. Upon indium doping, the *c*-axis expands as a result of the larger atomic radius of indium compared to that of Sn. This expansion increases both the interplanar spacing and the Tb–Mn interatomic distance, which may modify the electronic and magnetic properties of the material.[25,26,28,32–35] Temperature-dependent magnetization measurements for the parent compound ($x = 0$) reveal two distinct magnetic transitions: (i) an FIM transition near 435 K, corresponding to the onset of the FIM state with magnetic moments aligned in the *ab*-plane (FIM1), and (ii) a spin reorientation transition around 300 K, where the moments reorient to the *c*-axis direction (FIM2). With indium doping, the high-temperature FIM transition shifts to lower temperatures and eventually merges with the low-temperature spin reorientation transition at $x = 1.2$. The magnetic phase diagram (Fig. 1(c)) shows that the region of FIM1 progressively shrinks with increasing indium doping, ultimately disappearing at higher doping levels.

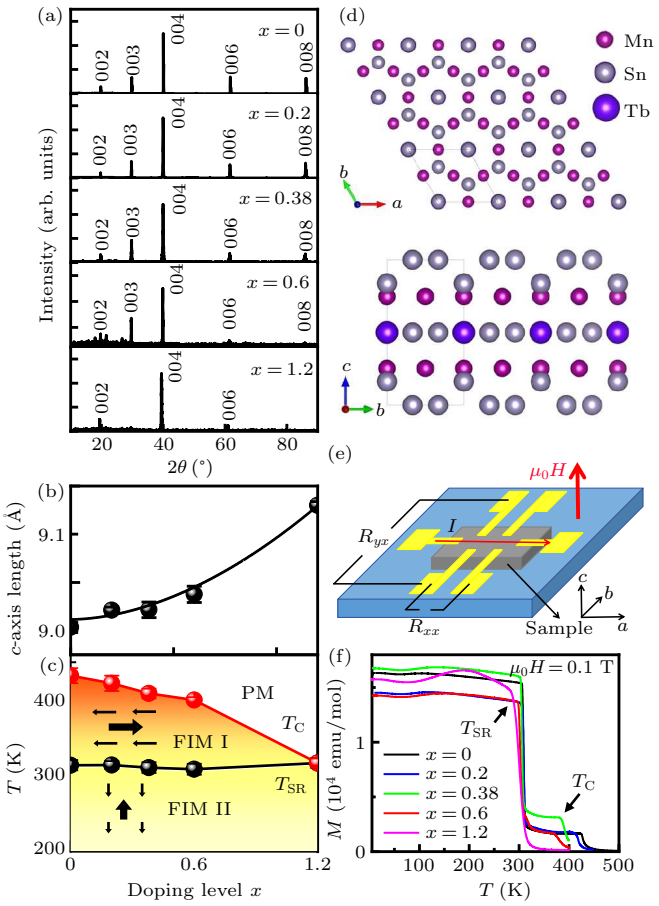


Fig. 1. (a) X-ray diffraction patterns for $TbMn_6Sn_{6-x}In_x$ ($x = 0$–1.2) at room temperature. (b) The crystal lattice constant *c* at various doping levels. (c) The phase diagram of $TbMn_6Sn_{6-x}In_x$. The FIM1 state, FIM2 state and paramagnetic state (PM) are labeled. (d) The schematic of the kagome layer of crystal structure for $TbMn_6Sn_6$. (e) The schematic measurement geometry. (f) Temperature dependence of magnetization for $TbMn_6Sn_{6-x}In_x$ ($x = 0$–1.2) with the applied field parallel to the *c*-axis.

To investigate the effect of indium doping, we first examine the magnetic and electronic transport properties in the low-temperature region. The field-dependent magnetization $M(\mu_0 H)$, along with Hall resistivity $\rho_{xy}(\mu_0 H)$ is shown in Fig. 2 for fields applied parallel to the *c*-axis. With indium doping, the saturated magnetic moment remains largely unchanged, particularly at low temperatures, in sharp contrast to those in $TbMn_6Ge_{6-x}Ga_x$.[36,37] This suggests that the introduction of nonmagnetic impurities causes minimal disruption to the magnetic structure, thus preserving the long-range magnetic order. In contrast, the Hall effect shows a strong depen-

dence on doping. At 100 K, $\rho_{xy}(\mu_0 H)$ increases systematically with the level of indium doping. In magnetic systems, the Hall effect typically arises from two contributions: (i) the ordinary Hall effect (OHE) due to the Lorentz force, and (ii) the anomalous Hall effect (AHE), which originates from magnetization or Berry curvature. The total Hall resistivity can be expressed as

$$\rho_{xy} = \rho_{xy}^{\mathrm{OHE}} + \rho_{xy}^{\mathrm{AHE}} = R_0 \mu_0 H + R_{\mathrm{A}} M, \quad (1)$$

where ρ_{xy}^{OHE}, and ρ_{xy}^{AHE} denote the ordinary Hall resistivity, and anomalous Hall resistivity respectively. R_0 and R_{A} are the ordinary Hall coefficient and the anomalous Hall coefficient, respectively.

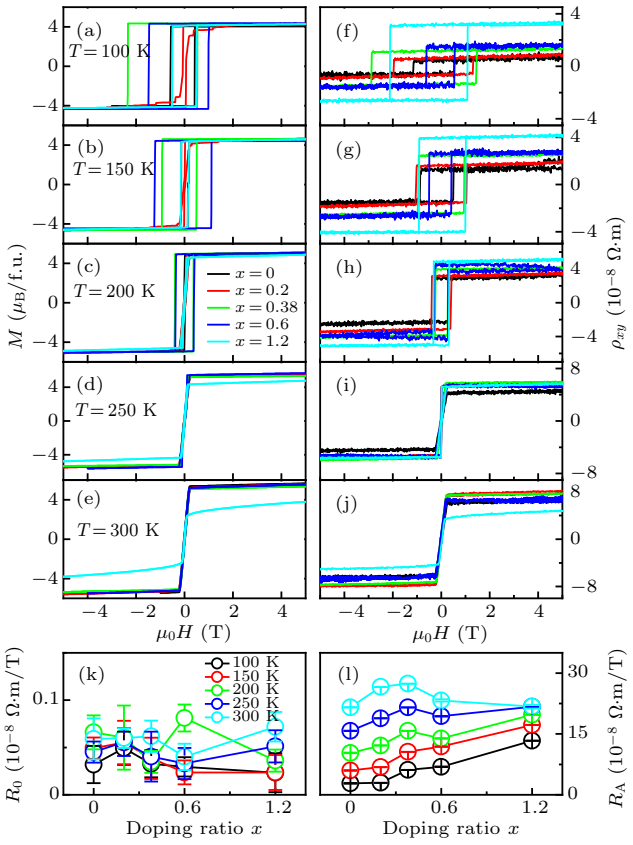


Fig. 2. Field dependence of magnetization and Hall resistivity at 100 K, 150 K, 200 K, 250 K, and 300 K for $TbMn_6Sn_{6-x}In_x$ ($x = 0$–1.2) are shown in panels (a)–(e) and (f)–(j) respectively. The doping dependence of ordinary Hall coefficient and anomalous Hall coefficient for $TbMn_6Sn_{6-x}In_x$ ($x = 0$–1.2) are shown in panels (k) and (l) respectively.

The doping dependence of R_0 and R_{A} at various temperatures are shown in Figs. 2(k) and 2(l). Indium doping does not significantly affect the carrier density, as indium has the same valence as Sn. While the variation in atomic size between Sn and indium could influence the carrier density, this change appears to be limited. In the low-temperature region, the anomalous Hall effect appears to increase roughly with doping. However, in the high-temperature region, especially near the spin reorientation transition, the anomalous Hall effect exhibits a non-monotonic evolution with doping due to increased magnetic fluctuations and short-range magnetic interactions. For $TbMn_6Sn_{6-x}In_x$ ($x = 1.2$), since the system approaches the paramagnetic state due to the absence of FIM1, the magnetization does not saturate with the applied field in the high temperature region (such as at 250 K and 300 K). Correspondingly, R_{A} of $TbMn_6Sn_{6-x}In_x$ ($x = 1.2$) demonstrates distinct temperature-dependent behavior compared to other compounds.[34]

To investigate the magnetic properties of $TbMn_6Sn_{6-x}In_x$ above room temperature, which is an important temperature range to evaluate its potential in high-temperature spintronics applications, field-dependent magnetization measurements were performed with the applied field aligned both along the *c*-axis and within the *ab*-plane (Fig. 3). We performed linear fitting on the saturated $M(\mu_0 H)$ parts of the curves to identify the transition region and then defined the saturation field $\mu_0 H_{\mathrm{sa}}$ as the point corresponding to 60% of the transition.

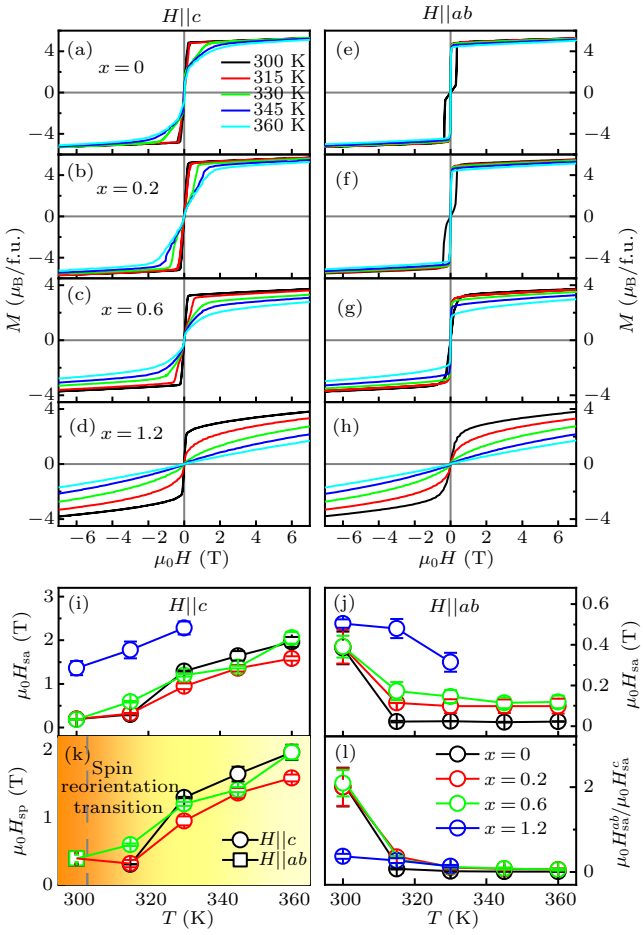


Fig. 3. Field dependence of magnetization at 300 K, 315 K, 330 K, 345 K, and 360 K for $TbMn_6Sn_{6-x}In_x$ ($x = 0$–1.2) with the applied field along the *c*-axis and the *ab*-plane are shown in panels (a)–(d) and (e)–(h), respectively. The saturated transition field $\mu_0 H_{\mathrm{sa}}$ acquired from panels (a)–(h) are shown with the applied field along the *c*-axis and the *ab*-plane are shown in panels (i) and (j). (k): The spin-flop transition field $\mu_0 H_{\mathrm{sp}}$ acquired from panels (a)–(h). The spin-flop transition emerges with the applied field perpendicular to the spontaneous magnetization direction. (l) The relative anisotropy of magnetization of $\mu_0 H_{\mathrm{sa}}$ for $TbMn_6Sn_{6-x}In_x$ ($x = 0$–1.2).

Above room temperature, following the spin reorientation transition, FIM1 gradually takes over the system, replacing FIM2 with the magnetization direction shifting from the *c*-axis toward the *ab*-plane. When the field is applied perpendicular to the spontaneous magnetization, the *M*–*H* loops display a two-step feature: a spin-flop transition ($\mu_0 H_{sp}$) followed by a magnetization saturation transition. As temperature increases, the saturation field ($\mu_0 H_{sa}$) increases when the field is aligned along the *c*-axis, while showing minimal variation when aligned parallel to the *ab*-plane. Notably, in $TbMn_6Sn_{6-x}In_x$ ($x = 1.2$), the absence of long-range magnetic order in this temperature range leads to a sharp increase in $\mu_0 H_{sa}$, as shown in Fig. 3. The relative anisotropy of magnetization, quantified by the ratio $\mu_0 H_{sa}^{ab}/\mu_0 H_{sa}^{c}$ (Fig. 3(l)), systematically decreases with increasing temperature while exhibits small variation with changing indium doping level.

In the following Fig. 4, we show the transport measurements of $TbMn_6Sn_{6-x}In_x$ in the high-temperature region. For the parent compound ($x = 0$), while saturation magnetization does not increase with temperature, the anomalous Hall resistivity continues to rise, reaching its peak value at 360 K. It is remarkable to observe such significant anomalous Hall contributions at this elevated temperature. The Hall effect demonstrates field dependence with a two-step feature, similar to the magnetization behavior when the field is applied along the same crystallographic direction. With indium doping, the anomalous Hall resistivity decreases, which is attributed to the shift of the transition temperature for long-range FIM order to lower temperatures. In $TbMn_6Sn_{6-x}In_x$ ($x = 1.2$), the anomalous Hall effect rapidly diminishes and completely disappears above 330 K. The transport properties of $TbMn_6Sn_{6-x}In_x$ exhibit a systematic evolution with both indium doping and increasing temperature.

Indium substitution not only alters the carrier density but also modifies the magnetic sublattice. In $TbMn_6Sn_6$, Mn–Mn and Mn–R interactions favor parallel alignment of the Mn moments, which is linked to ferromagnetic Tb–Tb interactions arising from the strong uniaxial anisotropy of the Tb^{3+} ions.[23] The second-order crystal electric field (CEF) further contributes to anisotropic magnetization.[7] Upon indium doping, the FIM ordering transition temperature decreases, and the Mn–Mn and RE–Mn interactions evolve systematically. The observed change in the easy magnetization direction in $TbMn_6Sn_{6-x}In_x$ compounds likely relates to the specific crystallographic site occupied by the Sn atoms. Substitutional indium alters the hyperfine field at the Sn sites,[32] which originates from three contributions: orbital, Fermi contact, and dipolar fields transferred from neighboring magnetic moments. Indium has a larger atomic radius compared to Sn, and its substitutional doping induces a systematic variation in the lattice, which alters the interaction of local moments. Ultimately, these effects result in a reduction of the hyperfine field observed at the Sn site. This hyperfine coupling is strongly affected by the rare-earth moments which leads to systemic evolution of magnetic state and anisotropy in $TbMn_6Sn_{6-x}In_x$.[8]

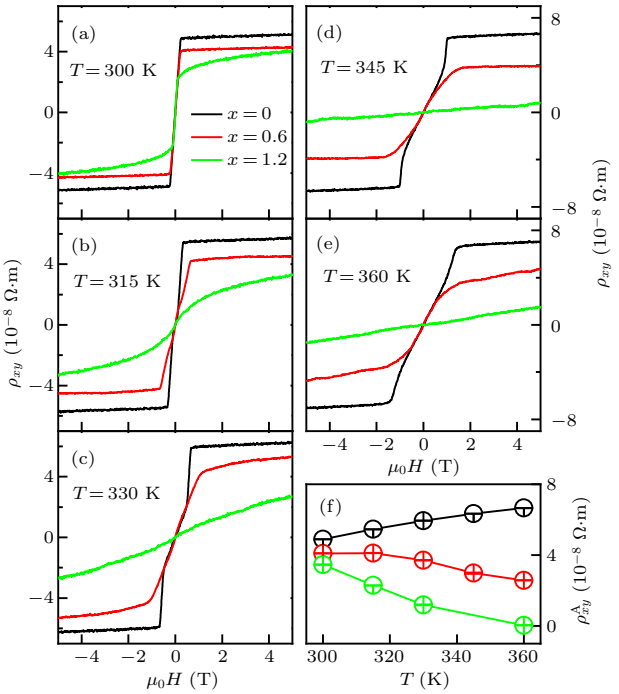


Fig. 4. (a)–(e) Field dependence of Hall resistivity (at 300 K, 315 K, 330 K, 345 K, 360 K for $TbMn_6Sn_{6-x}In_x$ ($x = 0$–1.2) with the applied field parallel to the *c*-axis. (f) Temperature dependence of anomalous Hall resistivity for $TbMn_6Sn_{6-x}In_x$ ($x = 0$–1.2).

The anomalous Hall effect shows a distinct evolution compared to magnetization, suggesting that indium doping likely affects the electron band topology and redistributes the Berry curvature. While indium doping appears to have minimal impact on the magnetic ground state of $TbMn_6Sn_{6-x}In_x$, it does influence the magnetic correlations, leading to changes in the magnetic transition temperature. Additionally, we note that, besides the long-range magnetic order, the short-range order also plays an important role in the electron band topology and Berry curvature.[38,39] These short-range orders emerge in a complex manner in $TbMn_6Sn_{6-x}In_x$ and are affected by defects due to indium doping.

At temperatures above 300 K, thermal occupancy of the isotropic state weakens the relative anisotropy of magnetization along the *c*-axis driving the spin-reorientation transition. In this region, indium doping leads to a rapid decrease in the anomalous Hall resistivity, attributed not only to reduced magnetization but also to suppression of the anomalous Hall coefficient. At the indium doping level of $x = 1.2$, the absence of long-range FIM order likely induces changes in Fermi topology, resulting in distinct Hall behavior compared to compounds at other doping levels. The systematic evolution of transport properties reflects significant modifications to both

magnetization and electron band structure caused by the indium substitution.

4. Conclusion

The systematic investigation of $TbMn_6Sn_{6-x}In_x$ ($x = 0$–1.2) kagome magnets reveals a profound interplay of chemical substitution, magnetic order, and electronic transport. These compounds exhibit a robust anomalous Hall effect that persists above room temperature, highlighting their potential for high-temperature spintronics applications.[40] At elevated temperatures, the emergence of an in-plane FIM1 state via a spin-flop transition correlates with a distinct non-monotonic Hall response, diverging from low-temperature behavior. Indium doping progressively suppresses the long-range FIM ordering temperature, reduces the relative anisotropy of magnetization along the *c*-axis compared to that within the *ab*-plane, and ultimately eliminates the FIM1 phase at $x = 1.2$. The suppression of magnetic phases and the tunability of the anomalous Hall effect emphasize the critical role of lattice–magnetism coupling in governing transport phenomena in kagome systems. The results underscore a coherent doping-driven evolution of magnetic and electronic states establishing $TbMn_6Sn_{6-x}In_x$ as a versatile material platform for designing high-temperature spintronics technologies.

Acknowledgements

Project supported by Guangzhou Basic and Applied Basic Research Foundation (Grant No. 2023B1515120013), the National Natural Sciences Foundation of China (Grant No. 92165204), the National Key Research and Development Program of China (Grant Nos. 2023YFF0718400 and 2022YFA1403301), the Fund from the Research Center for Magnetoelectric Physics of Guangdong Province, China (Grant No.2024B0303390001), and the Independent Fund of the State Key Laboratory of Optoelectronic & Materials and Technologies (Sun Yat-sen University) (Grant No. OEMT-2023-ZTS-01).

References

[1] Xu X T, Yin J X, Qu Z and Jia S 2023 *Rep. Prog. Phys.* **86** 114502
[2] Xiao D, Chang M C and Niu Q 2010 *Rev. Mod. Phys.* **82** 1959
[3] Li R S, Zhang T, Ma W L, Xu S X, Wu Q, Yue L, Zhang S J, Liu Q M, Wang Z X, Hu T C, Zhou X Y, Wu D, Dong T, Jia S, Weng H M and Wang N L 2023 *Phys. Rev. B* **107** 045115
[4] Riberolles S X M, Slade T J, Han T, Li B, Abernathy D L, Canfield P C, Ueland B G, Orth P P, Ke L and McQueeney R J 2024 *Nat. Commun.* **15** 1592
[5] Li L F, Chi S W, Ma W L, Guo K Z, Xu G and Jia S 2024 *Chin. Phys. B* **33** 057501
[6] Lyu M, Liu Y, Zhang S, Liu J, Yang J, Wang Y, Feng Y, Dong X, Wang B, Wei H and Liu E 2024 *Chin. Phys. B* **33** 107507
[7] Lee Y, Skomski R, Wang X, Orth P P, Ren Y, Kang B, Pathak A K, Kutepov A, Harmon B N, McQueeney R J, Mazin I I and Ke L 2023 *Phys. Rev. B* **108** 045132
[8] Perry L K, Ryan D H and Venturini G 2007 *Phys. Rev. B* **75** 144417
[9] Riberolles S X M, Slade T J, Abernathy D L, Granroth G E, Li B, Lee Y, Canfield P C, Ueland B G, Ke L and McQueeney R J 2022 *Phys. Rev. X* **12** 021043
[10] Wenzel M, Tsirlin A A, Iakutkina O, Yin Q, Lei H C, Dressel M and Uykur E 2022 *Phys. Rev. B* **106** L241108
[11] Venturini G, Idrissi B C E and Malaman B 1991 *J. Magn. Magn. Mater.* **94** 35
[12] Ma W, Xu X, Yin J X, Yang H, Zhou H, Cheng Z J, Huang Y, Qu Z, Wang F, Hasan M Z and Jia S 2021 *Phys. Rev. Lett.* **126** 246602
[13] Kimura S, Matsuo A, Yoshii S, Kindo K, Zhang L, Brück E, Buschow K H J, Boer F R, Lefèvre C and Venturini G 2006 *J. Alloys Compd.* **408–412** 169
[14] Annaberdiyev A, Mandal S, Mitas L, Krogel J T and Ganesh P 2023 *npj Quantum Mater.* **8** 50
[15] Huang D Q, Wang Y, Wang H, Wang J and Liu Y 2024 *Chin. Phys. Lett.* **41** 047801
[16] Yin J X, Ma W, Cochran T A, *et al.* 2020 *Nature* **583** 533
[17] Xu X, Yin J X, Ma W, Tien H J, Qiang X B, Reddy PVS, Zhou H, Shen J, Lu H Z, Chang T R, Qu Z and Jia S 2022 *Nat. Commun.* **13** 1197
[18] Zhang H, Koo J, Xu C, Sretenovic M, Yan B and Ke X 2022 *Nat. Commun.* **13** 1091
[19] Li Y, Graham RG, Bunbury DStP, Mitchell PW, McCausland MAH, Chaughule RS, Gupta LC, Vijayaraghavan R and Godart C 1995 *J. Magn. Magn. Mater.* **140–144** 1031
[20] Mielke III C, Ma W L, Pomjakushin V, *et al.* 2022 *Commun. Phys.* **5** 107
[21] El Idrissi B C, Venturini G, Malaman B and Fruchart D 1991 *J. Less-Common. Met.* **175** 143
[22] Huang Z, Wang W, Ye H, Bao S, Shangguan Y, Liao J, Cao S, Kajimoto R, Ikeuchi K, Deng G, Smidman M, Song Y, Yu S L, Li J X and Wen J 2024 *Phys. Rev. B* **109** 014434
[23] Riberolles S X M, Slade T J, Dally R L, Sarte P M, Li B, Han T, Lane H, Stock C, Bhandari H, Ghimire N J, Abernathy D L, Canfield P C, Lynn J W, Ueland B G and McQueeney R J 2023 *Nat. Commun.* **14** 2658
[24] Terent'ev P B and Mushnikov N V 2005 *Phys. Met. Metall.* **100** 571
[25] Chen X X, Zhao M, Liu G Z, Yao J L and Gao J 2016 *Int. J. Mod. Phys. B* **30** 1650068
[26] Hu J, Yang F, Wang J, Pan H, Zhao R, Tang N, Wang Y, Wang Z, Zhou K, Zhong X and de Boer F R 1997 *J. Appl. Phys.* **82** 760
[27] Terent'ev P B, Mushnikov N V, Gaviko V S, Shreder L A and Rosenfeld E V 2008 *J. Magn. Magn. Mater.* **320** 836
[28] Wang Y, Yang F, Chen C, Tang N, Han X and Wang Q 1996 *J. Phys.:L Condens. Matter* **8** 5737
[29] Wang Y G, Lin P, Chen C, Wang Q, Yang F and Tang N 1999 *J. Mater. Sci. Lett.* **18** 1123
[30] Wei Q, Zhou Y, Tan H, Gao L, Liu R, Jing J, Li Y, Chen D, Long Y Z, Li Q, Qi Y, Yan B, Teng B and Chen D 2025 *Phys. Rev. B* **111** 064412
[31] Zajkov N K, Mushnikov N V, Gerasimov E G, Gaviko V S, Bartashevich M I, Goto T and Khrabrov V I 2003 *J. Alloys Compd.* **363** 40
[32] Zhao P, Zhang S Y, Cheng Z H, Zhang H W, Sun J R, Shen B G and Dunlap R A 2001 *IEEE Trans. Magn.* **37** 2609
[33] Kong X M, Tao Z C, Zhang R, Xia W, Chen X, Pei C Y, Ying T P, Qi Y P, Guo Y F, Yang X F and Li S Y 2024 *Chin. Phys. Lett.* **41** 047503
[34] Lefèvre C and Venturini G 2002 *J. Alloys Compd.* **340** 6
[35] Lefèvre C, Venturini G and Malaman B 2003 *J. Alloys Compd.* **354** 47
[36] Xu H K, Li W J, Chen J J, Khmelevskyi S, Khalyavin D, Manuel P, Xi C Y, Kawaguchi S, Chen J, Yang W, Zhang Q H, Cao Y L, Yu C Y, Ren Y, Lin K and Xing X R 2025 *J. Am. Chem. Soc.* **147** 11941
[37] Yoshii S, Kindo K, Zhang L, Brück E, Buschow KHJ, De Boer FR, Lefèvre C and Venturini G 2006 *J. Alloys Compd.* **408** 173
[38] Wang B, Yi E, Li L, Qin J, Hu B F, Shen B and Wang M 2022 *Phys. Rev. B* **106** 125107
[39] Yi E K, Zheng D F, Pan F H, Zhang H X, Wang B, Chen B W, Wu D T, Liang H L, Mei Z X, Wu H, Yang S A, Cheng P, Wang M and Shen B 2023 *Phys. Rev. B* **107** 035142
[40] Li Z L, Yin Q W, Lv W X, Shen J, Wang S G, Zhao T Y, Cai J W, Lei H C, Lin S Z, Zhang Y and Shen B G 2024 *Adv. Mater.* **36** 2309538